Dynamics of Raman soliton during supercontinuum generation near the zero-dispersion wavelength of optical fibers

Samudra Roy,[1,*] Shyamal K. Bhadra,[2] Kunimasa Saitoh,[1] Masanori Koshiba,[1] and Govind P. Agrawal[3]

[1]*Graduate School of Information Science & Technology, Hokkaido University, Sapporo 060-0814, Japan*
[2]*Fiber Optics & Photonics Division, CGCRI, CSIR, Kolkata 700032, India*
[3]*Institute of Optics, University of Rochester, Rochester, New York 14627, USA*
**samudraroy@yahoo.co.in*

Abstract: We observe unique dynamics of Raman soliton during supercontinuum process when an input pulse experiences initially normal group-velocity dispersion with a negative dispersion slope. In this situation, the blue components of the spectrum form a Raman soliton that moves faster than the input pulse and eventually decelerates because of Raman-induced frequency downshifting. In the time domain, the soliton trajectory bends and becomes vertical when the Raman shift ceases to occur as the spectrum of Raman soliton approaches the zero dispersion point. Parts of the red components of the pulse spectrum are captured by the Raman soliton through cross-phase modulation and they travel with it. The influence of soliton order, input chirp and dispersion slope on the dynamics of Raman soliton is discussed thoroughly.

OCIS codes: (190.0190) Nonlinear Optics; (190.5530) Pulse propagation and temporal solitons.

References and links

1. J. M. Dudley, G. Genty, and S. Coen, "Supercontinuum generation in photonics crystal fiber," Rev. Mod. Phys. **78**(4), 1135–1184 (2006).
2. R. Holzwarth, T. Udem, T. W. Hansch, J. C. Knight, W. J. Wadsworth, and P. St. J. Russell, "Optical frequency synthesizer for precision spectroscopy," Phys. Rev. Lett. **85**(11), 2264–2267 (2000).
3. S. Smirnov, J. D. Ania-Castanon, T. J. Ellingham, S. M. Kobtsev, S. Kukarin, and S. K. Turitsyn, "Optical spectral broadening and supercontinuum generation in telecom applications," Opt. Fiber Technol. **12**(2), 122–147 (2006).
4. G. P. Agrawal, *Nonlinear Fiber Optics*, 4th ed. (Academic Press, 2007).
5. J. M. Dudley and J. R. Taylor, *Supercontinuum Generation in Optical Fibers* (Cambridge University Press, 2010).
6. A. V. Gorbach, D. V. Skryabin, J. M. Stone, and J. C. Knight, "Four-wave mixing of solitons with radiation and quasi-nondispersive wave packets at the short-wavelength edge of a supercontinuum," Opt. Express **14**(21), 9854–9863 (2006).
7. G. Genty, M. Lehtonen, and H. Ludvigsen, "Effect of cross-phase modulation on supercontinuum generated in microstructured fibers with sub-30 fs pulses," Opt. Express **12**(19), 4614–4624 (2004).
8. N. Akhmediev and M. Karlsson, "Cherenkov radiation emitted by solitons in optical fibers," Phys. Rev. A **51**(3), 2602–2607 (1995).
9. A. V. Husakou and J. Herrmann, "Supercontinuum generation of higher-order solitons by fission in photonic crystal fibers," Phys. Rev. Lett. **87**(20), 203901 (2001).
10. J. Dudley, X. Gu, L. Xu, M. Kimmel, E. Zeek, P. O'Shea, R. Trebino, S. Coen, and R. Windeler, "Cross-correlation frequency resolved optical gating of the broadband continuum generation in photonics crystal fibers: simulations and experiments," Opt. Express **10**(21), 1215–1221 (2002).
11. V. I. Karpman, "Radiation by solitons due to higher-order dispersion," Phys. Rev. E Stat. Phys. Plasmas Fluids Relat. Interdiscip. Topics **47**(3), 2073–2082 (1993).
12. A. V. Gorbach and D. V. Skryabin, "Light trapping in gravity-like potentials and extension of supercontinuum spectra in photonic crystal fibers," Nat. Photonics **1**(11), 653–657 (2007).
13. D. V. Skryabin and A. V. Gorbach, "Colloquium: Looking at a soliton through the prism of optical supercontinuum," Rev. Mod. Phys. **82**(2), 1287–1299 (2010).

#142719 - $15.00 USD Received 16 Feb 2011; accepted 4 May 2011; published 12 May 2011

14. S. Roy, S. K. Bhadra, and G. P. Agrawal, "Effects of higher-order dispersion on resonant dispersive waves emitted by solitons," Opt. Lett. **34**(13), 2072–2074 (2009).
15. P. St. J. Russell, "Photonic crystal fibers," Science **299**(5605), 358–362 (2003).
16. W. H. Reeves, D. V. Skryabin, F. Biancalana, J. C. Knight, P. St. J. Russell, F. G. Omenetto, A. Efimov, and A. J. Taylor, "Transformation and control of ultra-short pulses in dispersion-engineered photonic crystal fibres," Nature **424**(6948), 511–515 (2003).
17. K. Saitoh, N. Florous, and M. Koshiba, "Ultra-flattened chromatic dispersion controllability using a defected-core photonic crystal fiber with low confinement losses," Opt. Express **13**(21), 8365–8371 (2005).
18. Q. Lin and G. P. Agrawal, "Raman response function for silica fibers," Opt. Lett. **31**(21), 3086–3088 (2006).
19. N. Joly, F. Omenetto, E. Efimov, A. Taylor, J. C. Knight, and P. St. J. Russell, "Competition between spectral splitting and Raman frequency shift in negative-dispersion slope photonics crystal fiber," Opt. Commun. **248**(1-3), 281–285 (2005).
20. S. Roy, D. Ghosh, S. K. Bhadra, and G. P. Agrawal, "Role of dispersion profile in controlling the emission of dispersive waves by solitons in supercontinuum generation," Opt. Commun. **283**(15), 3081–3088 (2010).
21. D. V. Skryabin, F. Luan, J. C. Knight, and P. St. J. Russell, "Soliton self-frequency shift cancellation in photonic crystal fibers," Science **301**(5640), 1705–1708 (2003).
22. M. Erkintalo, G. Genty, and J. M. Dudley, "Experimental signatures of dispersive waves emitted during soliton collisions," Opt. Express **18**(13), 13379–13384 (2010).
23. K. C. Chan and H. F. Liu, "Effects of Raman scattering and frequency chirping on soliton-effect pulse compression," Opt. Lett. **18**(14), 1150–1152 (1993).
24. E. N. Tsoy and C. M. de Sterke, "Dynamics of ultrashort pulses near zero dispersion wavelength," J. Opt. Soc. Am. B **23**(11), 2425–2433 (2006).
25. J. Herrmann, U. Griebner, N. Zhavoronkov, A. Husakou, D. Nickel, J. C. Knight, W. J. Wadsworth, P. St. J. Russell, and G. Korn, "Experimental evidence of supercontinuum generation by fission of higher order solitons in photonics crystal fibers," Phys. Rev. Lett. **88**(17), 173901 (2002).
26. J. M. Dudley, L. Provino, N. Grossard, H. Maillotte, R. S. Windeler, B. J. Eggleton, and S. Coen, "Supercontinuum generation in all-silica microstructured fibers with nanosecond and femtosecond pulse pumping," J. Opt. Soc. Am. B **19**(4), 765–771 (2002).
27. A. V. Gorbach and D. V. Skryabin, "Theory of radiation trapping by accelerating solitons in optical fibers," Phys. Rev. A **76**(5), 053803 (2007).
28. G. Genty, M. Lehtonen, and H. Ludvigsen, "Route to broadband blue-light generation in microstructured fibers," Opt. Lett. **30**(7), 756–758 (2005).
29. G. Genty, M. Lehtonen, H. Ludvigsen, and M. Kaivola, "Enhanced bandwidth of supercontinuum generated in microstructured fibers," Opt. Express **12**(15), 3471–3480 (2004).
30. F. Biancalana, D. V. Skryabin, and A. V. Yulin, "Theory of the soliton self-frequency shift compensation by the resonant radiationin photonic crystal fibers," Phys. Rev. E Stat. Nonlin. Soft Matter Phys. **70**(1), 016615 (2004).
31. S. Roy, S. K. Bhadra, and G. P. Agrawal, "Dispersive waves emitted by solitons perturbed by third-order dispersion inside optical fibers," Phys. Rev. A **79**(2), 023824 (2009).

1. Introduction

Supercontinuum (SC) generation in photonics crystal fibers (PCF) [1] has attracted considerable attention in recent years because of its wide applications ranging from spectroscopy and metrology [2] to telecommunications [3]. Extensive studies reveal that several physical phenomena are involved in the process of SC generation [4,5] when an ultrashort optical pulse experiences anomalous dispersion and undergoes enormous spectral broadening during its propagation inside a PCF. Self-phase modulation (SPM), intrapulse Raman scattering (IPRS) [4], four wave mixing [6], cross-phase modulation (XPM) [7], modulation instability [4], and dispersive wave (DW) generation [8] are the major nonlinear processes that take part actively during SC generation.

The interplay between the dispersion and nonlinearity of the waveguide produces optical solitons whose dynamics play a pivotal role in the process of SC generation when an ultrashort optical pulse is launched in the anomalous group-velocity dispersion (GVD) domain. In particular, the ideal periodic evolution of a higher-order soliton is perturbed by third- and higher-order dispersions (HOD) to the extent that it breaks into its fundamental components, a phenomenon known as soliton fission [9]. These fundamental solitons experience IPRS-induced red shifts, and this shift is largest for the shortest soliton with the highest peak power, also called the Raman soliton [4,10]. During the fission process, HOD terms lead to transfer of energy from the soliton to a narrowband resonant DW, also called non-solitonic radiation [8,9,11]. This DW is emitted on the blue side of the original pulse

#142719 - $15.00 USD Received 16 Feb 2011; accepted 4 May 2011; published 12 May 2011

spectrum for positive values of third-order dispersion and is of considerable practical importance for generating blue-shifted radiation. The interaction between the soliton and the DW turns out to be quite interesting and it has been studied extensively in recent years with an analogy to gravity-like potential [12,13].

It is well known that dispersive properties of the PCF play a governing role in producing the DW and controlling the SC generation [14]. Recent developments in PCF technology [15] have made it possible to observe new regimes of nonlinear pulse propagation because such fibers exhibit fascinating dispersion profiles with enhanced nonlinearities. An appropriate design of a PCF not only shifts the zero dispersion (ZD) wavelength toward shorter wavelengths but also produces dispersion profiles with multiple ZD points, features unattainable with conventional fibers [16,17]. Unusual soliton dynamics are expected when an ultrashort optical pulse is launched in the vicinity of a ZD point since the broadened pulse spectrum experiences opposite types of dispersion across the ZD point. In this study, new features are revealed when a femtosecond pulse is launched in the normal GVD region with a monotonous dispersion slope, a situation not explored in detail previously. We first qualitatively discuss soliton dynamics in the light of group delay curve when input pulse is launched exactly at the ZD wavelength. Next, we change the launch condition by detuning the pulse in the vicinity of the ZD point and explore pulse dynamics under both the positive and negative dispersion slopes. For a negative value of third-order dispersion (TOD), the Raman soliton is formed by the blue components of the pulse falling in the anomalous-GVD regime and it exhibits unusual dynamics by pulling its counterpart in the red region of the spectrum. In the case of a positive TOD, optical soliton is formed by the red components of the pulse and is found to interact with its counterpart via XPM during propagation inside the PCF, resulting in a spectral pushing. The influence of soliton order, input chirp, and dispersion slope on the pulse dynamics is studied extensively with multiple numerical examples.

2. Theory

To capture the dynamics of SC generation in the vicinity of the ZD wavelength, we solve the generalized nonlinear Schrödinger equation (GNLSE) written in its normalized form as [4]

$$\frac{\partial U}{\partial \xi}+\sum_{m=2}^{\infty} i^{m-1}\delta_m \frac{\partial^m U}{\partial \tau^m}=iN^2\left(1+is\frac{\partial}{\partial \tau}\right)\left(U(\xi,\tau)\int_{-\infty}^{\tau} R(\tau-\tau')\left|U(\xi,\tau')\right|^2 d\tau'\right) \quad (1)$$

where the field amplitude $U(\xi, \tau)$ is normalized such that $U(0, 0) = 1$. The other dimensionless quantities are defined as

$$\xi=\frac{z}{L_D},\ \tau=\frac{t-z/v_g}{T_0},\ N=\sqrt{\gamma P_0 L_D},\ \delta_m=\frac{\beta_m}{m!T_0^{m-2}\left|\beta_2\right|}. \quad (2)$$

Here, P_0 is the peak power of the ultrashort pulse launched into the fiber, T_0 is related to its width, $L_D=T_0^2/\left|\beta_2\right|$ is the dispersion length, v_g is the group velocity, γ is the nonlinear parameter, δ_m is the m^{th} order dispersion coefficient in normalized form, $s=(2\pi\nu_0 T_0)^{-1}$ is the self-steepening parameter at the carrier frequency ν_0 of the pulse, and $R(\tau)$ is the nonlinear response function in the form

$$R(\tau)=(1-f_R)\delta(\tau)+f_R h_R(\tau), \quad (3)$$

where f_R = 0.245 and the first and the second terms correspond to the electronic and Raman responses, respectively. As discussed in Ref. [18], the Raman response function can be expressed in the form,

#142719 - $15.00 USD Received 16 Feb 2011; accepted 4 May 2011; published 12 May 2011

$$h_R(\tau) = (f_a + f_c)h_a(\tau) + f_b h_b(\tau), \tag{4}$$

where the functions $h_a(\tau)$ and $h_b(\tau)$ are defined as

$$h_a(\tau) = \frac{\tau_1^2 + \tau_2^2}{\tau_1 \tau_2^2} \exp\left(-\frac{\tau}{\tau_2}\right) \sin\left(\frac{\tau}{\tau_1}\right),$$
$$h_b(\tau) = \left(\frac{2\tau_b - \tau}{\tau_b^2}\right) \exp\left(-\frac{\tau}{\tau_b}\right), \tag{5}$$

and the coefficients f_a = 0.75, f_b = 0.21, and f_c = 0.04 quantify the relative contributions of the isotropic and anisotropic parts of the Raman response. In Eq. (5), τ_1, τ_2 and τ_b have values of 12, 32 and 96 fs, respectively. In our notation, they have been normalized by the input pulse width T_0.

3. Numerical results

We employ the standard split-step Fourier method [4] to solve the GNLSE numerically. Since we work in normalized units, we do not need to specify the input wavelength. In the case of a PCF with two widely separated ZD wavelengths, it can be applied near the either ZD point by choosing the two dispersion parameters δ_2 and δ_3 appropriately. Note that in our notation δ_2 has a fixed value of ± 0.5, depending on whether the input pulse wavelength lies in the normal or anomalous GVD region. The parameter δ_3 can also take positive or negative values. The input pulse with the field $U(0, t)$ = sech(t/T_0) is assumed to have T_0 = 50 fs (full width at half maximum of about 88 fs). For a chirped pulse, the input field is of the form $U(0,\tau) = \text{sech}(\tau)\exp(-iC\tau^2)$, C being the normalized chirping parameter. The peak power of the input pulse is chosen such that the soliton order N takes different values ranging from 4 to 10, and the maximum fiber length corresponds to five dispersion lengths (ξ varies from 0 to 5). Self-steepening effects are negligible in our simulations because $s < 0.02$ for T_0 = 50 fs at a wavelength of 1550 nm. Thus, IPRS is the major higher-order nonlinear process affecting the launched pulse in addition to the SPM. In our simulations we employ a constant dispersion slope with all HOD terms set to zero. This amounts to assuming $\beta_2 = \beta_3 (\omega - \omega_{zd})$ over the entire SC range where ω_{zd} is the zero dispersion frequency. Such a specific dispersion profile can be realized with small core diameter of PCFs as discussed in Ref. [19].

3.1 Input pulse launched in the normal GVD region

Our objective is to investigate the role of dispersion slope or TOD on pulse dynamics under different launch condition. Pulse evolution is significantly influenced by the numerical sign of TOD coefficient. For $\delta_3 > 0$, a DW is generated on the blue side and it travels slower than the Raman soliton. Exactly opposite happens for $\delta_3 < 0$, that is, the DW is generated on the red side and travels faster than the Raman soliton [20]. The relative speeds of different spectral components of the pulse, as compared to the input pulse speed, is governed by the frequency-dependent group delay defined as

$$\delta_1(x) = \sum_{m=1}^{\infty} \frac{(m+1)!}{m!} \delta_{m+1} x^m \tag{6}$$

where $x = (\omega - \omega_0)T_0$ is the normalized frequency. In our case the series includes only m = 1 and m = 2 terms, and we have a simple parabolic relationship. In Eq. (6) shows that, all

#142719 - $15.00 USD Received 16 Feb 2011; accepted 4 May 2011; published 12 May 2011

objects travel slower than the incident pulse for $\delta_3 > 0$ when pulse is launched close to the ZD point. Exactly opposite happens when the sign of δ_3 is changed.

Although SC generation in the case of anomalous GVD has been studied extensively, much less attention has been paid to the case of normal GVD. In this section we consider the case in which a femtosecond optical pulse is launched in the normal-dispersion region but relatively close to the ZD point to ensure that the high and low frequency components of the broadened pulse spectrum experience opposite types of dispersions during propagation. We allow δ_3 to take positive or negative values since its sign plays an important role.

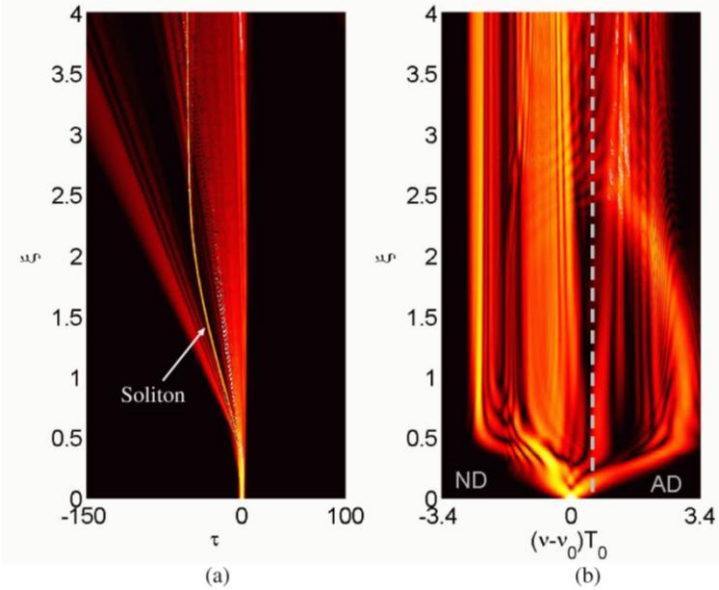

Fig. 1. (a) Temporal and (b) spectral evolution of an optical pulse launched in the normal dispersion (δ_2 = 0.5) domain close to the ZD wavelength with N = 8 and δ_3 = –0.05. The vertical dotted line indicates the ZD point.

Consider first the case of negative TOD ($\delta_3 < 0$). Figure 1 shows the temporal and spectral evolutions over 4 dispersion lengths using N = 8. . Soon after the pulse spectrum broadens owing to SPM, the blue and red parts of the pulse see opposite types of GVDs. In the present case, blue components of the pulse experience anomalous GVD, whereas red components lie in the normal-GVD region. Thus, the blue part of the spectrum forms a higher order soliton that undergoes the fission process near ξ = 0.5. After the fission, all spectral components of the pulse travel faster than the original pulse, as seen clearly Fig. 1(a), including the DW generated during fission process. This can be understood by noting that the group velocity increases on both sides of the ZD point for $\delta_3 < 0$. An interesting feature seen in Fig. 1(a) is the unusual trajectory of the Raman soliton. While the soliton is initially accelerated (a negative delay), after a certain distance it starts to slow down and eventually moves at a constant speed. This behavior is a consequence of IPRS-induced red shift of the soliton seen in Fig. 1(b) and its eventual cancellation after ξ = 2. Notice how the dominant blue peak associated with the Raman soliton gradually shifts to lower frequencies and then stops shifting. This behavior is consistent with what was observed experimentally in Ref. [19]. Physically speaking, as the soliton shifts towards longer wavelengths because of IPRS [4], it begins to slow down. This deceleration appears as a bending of its trajectory in the time domain. After ξ = 2, it moves at a constant speed (close to that of the input pulse) because the Raman shift is cancelled as the soliton approaches the ZD point. This spectral recoiling phenomenon was first observed in a PCF with two ZD wavelengths when the input pulse

#142719 - $15.00 USD Received 16 Feb 2011; accepted 4 May 2011; published 12 May 2011

launched near the shorter-wavelength ZD point created a SC broad enough to encompass the longer-wavelength ZD point [21]. Our work shows that it can also happen when we launch the input pulse in the normal GVD region near the second ZD point and does not require the formation of a very wide SC.

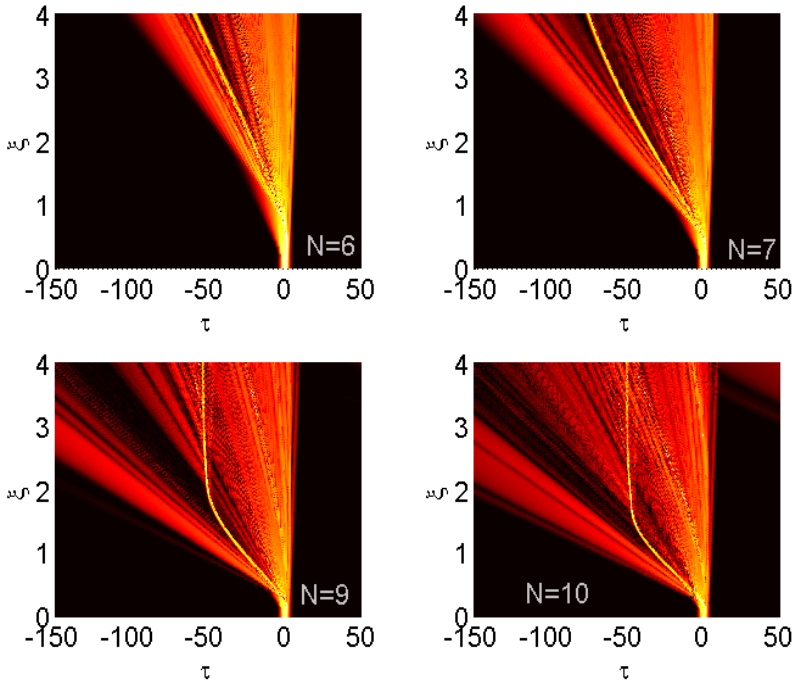

Fig. 2. Temporal evolution for four different values of N ranging from 6 to 10. Other parameters are identical to those used in Fig. 1.

Bending of the soliton trajectory depends considerably on the peak power of the input pulse because it sets the order of the soliton that undergoes the fission process. Numerical simulations shown in Fig. 2 reveal that bending of the temporal trajectory occurs earlier and quicker with increasing values of N. This is expected because IPRS increases with the soliton order, producing larger red shifts. The DW on the other hand accelerates rapidly with increasing soliton order. Since DW never overlaps with the Raman soliton, it is not trapped by this soliton. These features are clearly seen in Fig. 2 where we show temporal evolution for values of N up to 10 with $\delta_3 = -0.05$.

#142719 - $15.00 USD Received 16 Feb 2011; accepted 4 May 2011; published 12 May 2011

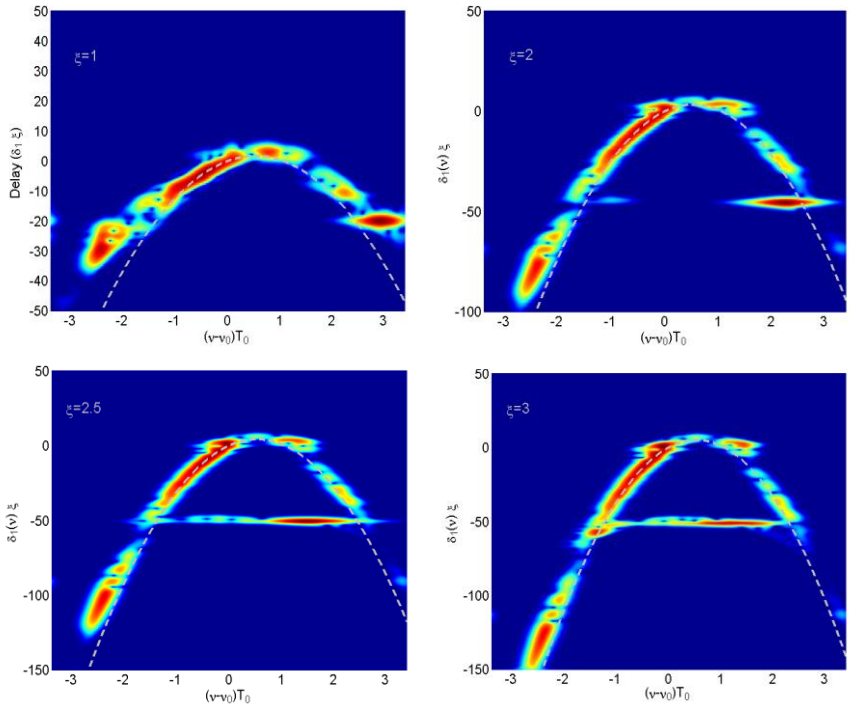

Fig. 3. Spectrograms of the pulse at four different lengths for parameter values identical to those used in Fig. 1. The dotted curves represent the time delay (δ_1 ξ).

The spectrograms shown in Fig. 3 at four different distances for N = 8 reveal a clearer picture of the entire process. The dashed curve in each case shows the time delay. The dominant soliton initially accelerates but its position stops shifting after ξ = 2. Although it does not overlap with the DW, it captures other red spectral components that overlap with it in the time domain. The XPM interaction between the two results in chirping, which shifts the soliton spectrum toward red and the spectrum of the non-soliton part toward blue. The spectrograms in Fig. 3 capture this spectral shifting process and reveal a kind of spectral attraction between the soliton and the trapped part moving together as one unit.

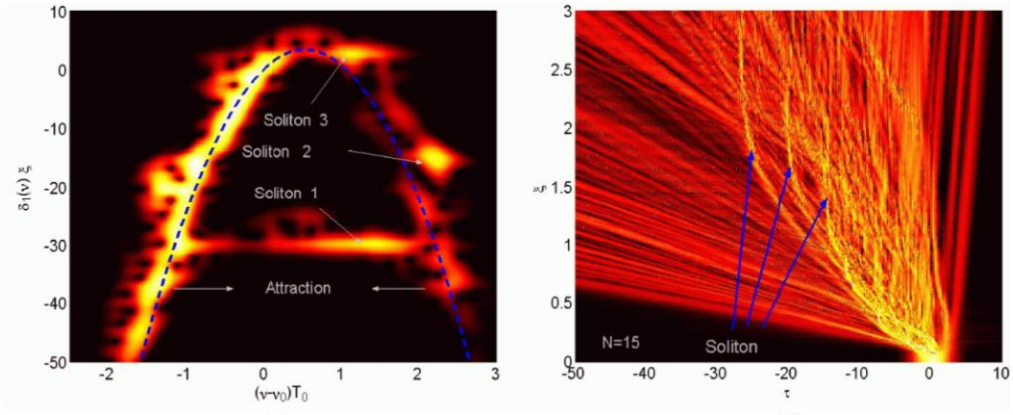

Fig. 4. (a) Spectrogram at a distance ξ = 2 for N = 10 and δ_3 = –0.05. The dotted curve represents the delay. (b) Temporal evolution for N = 15 and δ_3 = –0.05.

#142719 - $15.00 USD Received 16 Feb 2011; accepted 4 May 2011; published 12 May 2011

With increasing soliton order, several Raman solitons may form during the soliton fission process [4,9]. As an example, the spectrogram for the propagation of a 10th order soliton is shown in Fig. 4(a) where we see three distinct solitons are generated. In the case of anomalous GVD, for $N = 10$ one can expect the formation of 10 different solitons after the fission process [4]. In the present case, the optical pulse is launched in the normal-GVD domain, and only a fraction of pulse energy lies in the anomalous region because of spectral broadening. This reduces the number of solitons that can be created during the fission process. It is interesting to note that, among the three solitons, only the shortest soliton [soliton 1 in Fig. 4(a)] captures the red components of the pulse and forces them to move with it. This is because this Raman soliton shifts most toward red through IPRS. For still larger values of N, we expect that other solitons will also trap red components of the pulse. As seen in Fig. 4(b) for $N = 15$, the trajectory of several solitons bends as each one undergoes deceleration induced by IPRS. It should be noticed that not only the number of DWs is increased with increasing N, but new DWs are also generated because of the collision of solitons [22].

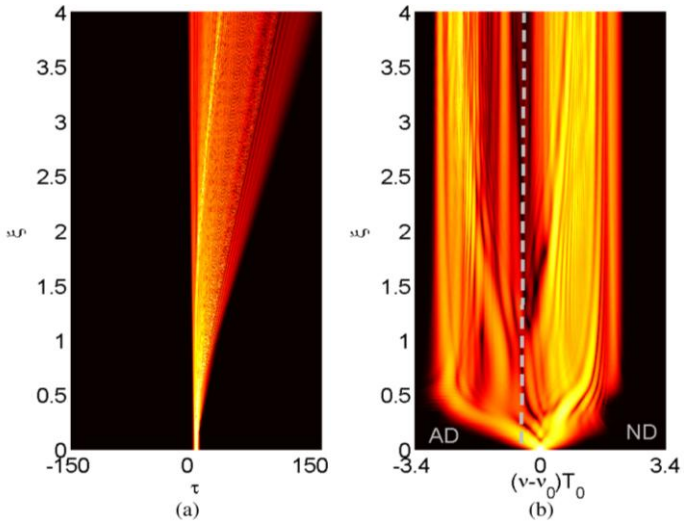

Fig. 5. (a) Temporal and (b) spectral evolution under conditions identical to those of Fig. 1 except that the sign of TOD is reversed ($\delta_3 = 0.05$).

Next, we consider the propagation near a ZD point with positive TOD. Except for changing the sign of δ_3, all other parameters are kept the same to facilitate comparison. In contrast to the previous case, now optical soliton is generated by the low-frequency components (red part) of the spectrum, as shown in Fig. 5. However, a significant amount of pulse energy lies in the blue part falling in the normal-GVD domain. Figure 5 should be compared with Fig. 1 because only difference between the two is the sign of δ_3. The main difference in the case of positive TOD is that the Raman soliton never approaches the ZD point as its spectrum shifts toward the red. This difference is responsible for very different temporal and spectral evolutions seen in the two cases. In particular, we can see Raman soliton is delayed more and more with propagation as its spectra shifts toward the red side. The DW is delayed even more and is not captured by this soliton. With increasing soliton order, the fraction of input pulse energy falling in the AD domain increases. Figure 6 is similar to Fig. 2 with the only difference that the sign of TOD is reversed. We can see formation of multiple solitons for large N, and the temporal delay increases with increasing soliton order.

#142719 - $15.00 USD Received 16 Feb 2011; accepted 4 May 2011; published 12 May 2011

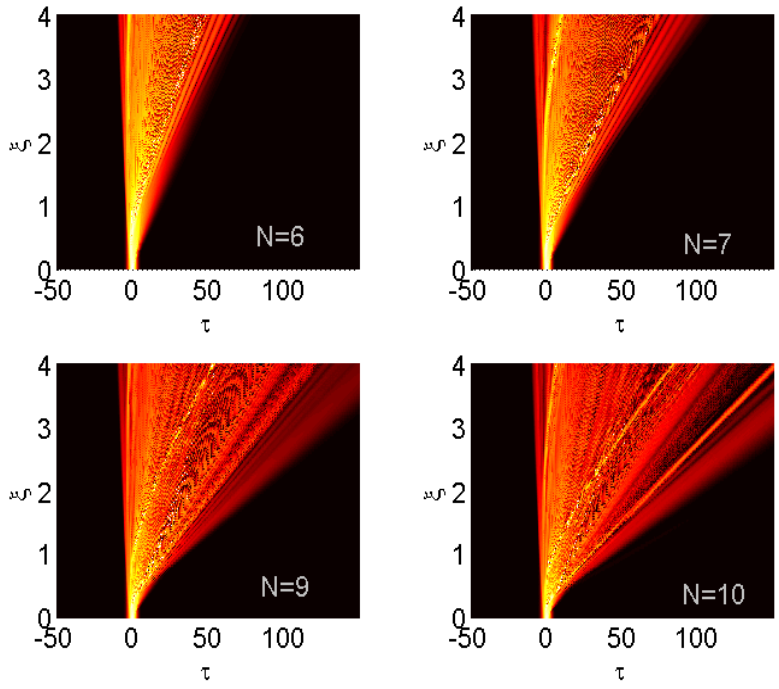

Fig. 6. Temporal evolution for four different values of N ranging from 6 to 10. Other parameters are identical to those used in Fig. 5.

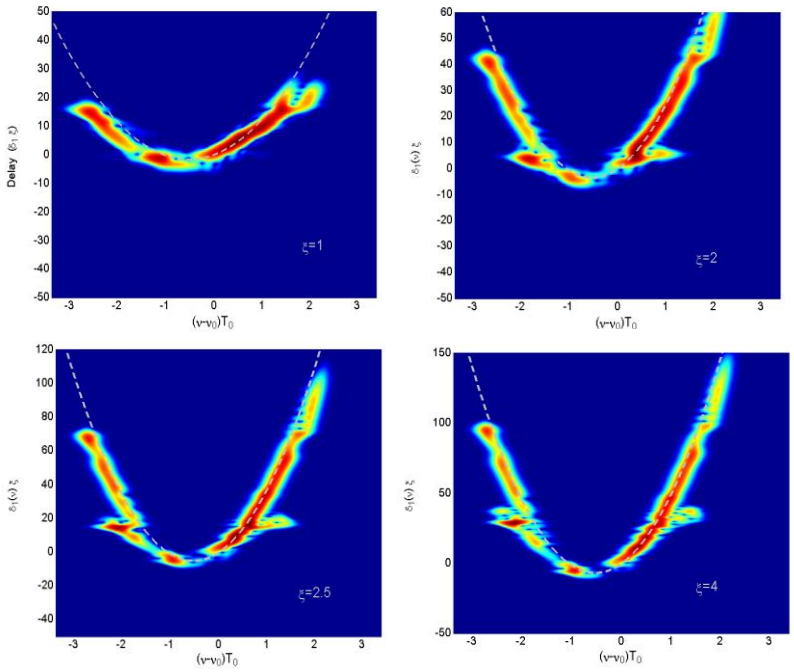

Fig. 7. Spectrograms of the pulse at four different lengths for parameter values identical to those used in Fig. 5. The dotted curves represent the delay.

The spectrograms in Fig. 7 are the counterparts of those in Fig. 3. As shown in the Fig. 7, the soliton generated by the red components of the pulse interacts with the radiation on the

#142719 - $15.00 USD Received 16 Feb 2011; accepted 4 May 2011; published 12 May 2011

blue side that overlaps with it in the time domain via the XPM process, and new frequency components are generated through chirping. As the soliton shifts toward red, it forces the non-soliton part to shift toward blue so that the two can move at the same speed. In the spectrogram representation, this event appears as a kind of spectral repulsion, exactly opposite of what we observe in Fig. 3. This behavior is shown more clearly in Fig. 8 for N = 10. Two solitons are captured in this figure, and both of them trap blue components and exhibit spectral repulsion.

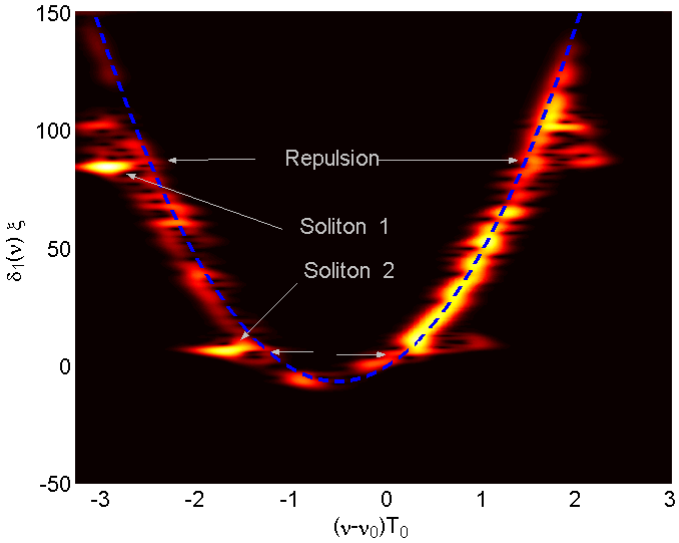

Fig. 8. Spectrogram at a distance $\xi = 2$ for N = 10 and $\delta_3 = 0.05$.The dotted curve represents the delay.

We briefly consider the effect of input chirp on the SC process. Figure 9 shows the temporal and spectral evolution of a 8th-order soliton for three values of the chirp parameter ranging from –1 to 1. It is evident that input chirp has a significant effect on pulse dynamics. With increasing chirp, bending of the Raman soliton in the time domain increases. This feature is also reflected in the spectral evolution. The soliton spectrum on the blue side belonging to the Raman soliton begins to turn more rapidly towards the red side with increasing frequency chirp. As chirp increases, the pulse reaches the fission stage earlier and earlier [23]. Because of this, the influence of IPRS increases for positive chirp and it bends the pulse earlier in the time domain. Exactly opposite phenomenon happens for a negative input chirp and we observe less bending.

#142719 - $15.00 USD Received 16 Feb 2011; accepted 4 May 2011; published 12 May 2011

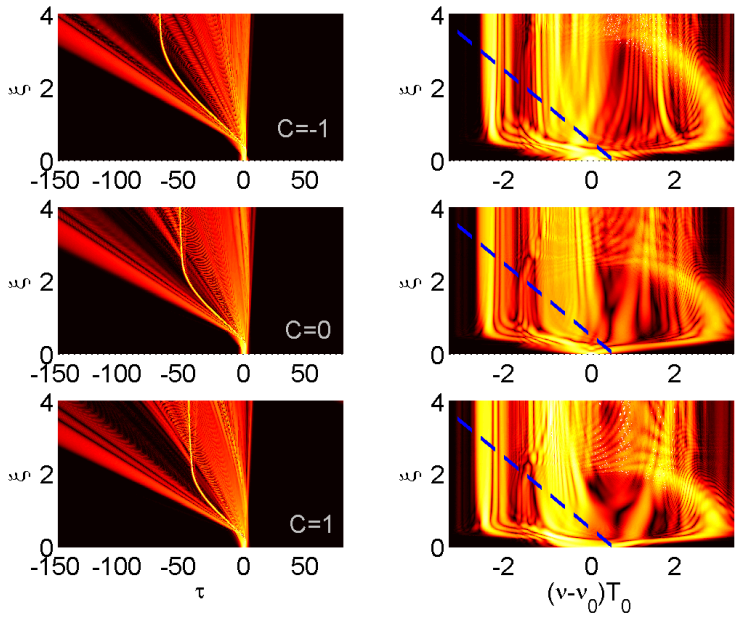

Fig. 9. Temporal (left column) and spectral (right column) evolution under conditions identical to those used in Fig. 1 except that the chirp parameter takes values from –1 to 1 . The blue dotted lines show δ_2 as function of normalized frequency.

So far we have investigated the pulse dynamics for a fixed value of the TOD coefficient ($\delta_3 = \pm 0.05$). As we saw, increasing the soliton order or a positive input chirp increases the bending of the Raman soliton in the time domain. The numerical value of TOD is another factor which influences this bending significantly. Figure 10 shows the temporal and spectral evolutions of a 8th-order soliton for four negative values of δ_3. As expected, the larger the absolute value of δ_3, the earlier the soliton trajectory bends. Figure 10(b) shows the corresponding changes in pulse spectra. With increasing TOD coefficient, the rate of IPRS increases and the soliton approaches the ZD point at a shorter distance along the fiber.

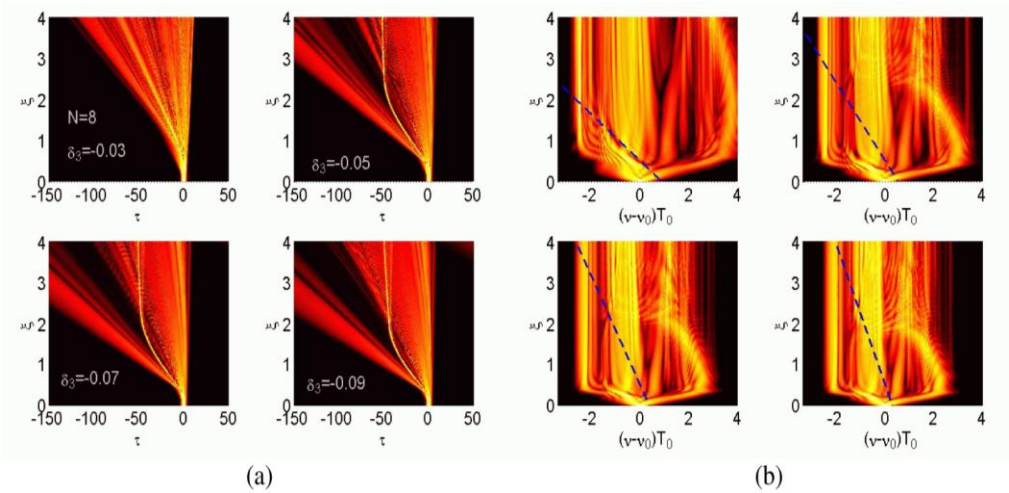

Fig. 10. (a) Temporal (two left columns) and (b) spectral (two right columns) evolution under conditions identical to those used in Fig. 1 except that the TOD parameter takes four different values ranging from –0.03 to –0.09. The blue dotted lines show δ_2 as function of normalized frequency.

#142719 - $15.00 USD Received 16 Feb 2011; accepted 4 May 2011; published 12 May 2011

3.2 Input pulse launched at the anomalous GVD region

In this section we study the situation when an optical pulse is launched in the anomalous-GVD domain (but very close to the ZD point) and allow positive and negative values of TOD. The case of positive TOD has been explored extensively in the past [24–29]. In particular, trapping of the DW by a Raman soliton has been studied extensively [27–29]. The case of negative δ_3 has also been studied in the context of IPRS cancellation in PCFs having two ZD wavelengths [21,30].

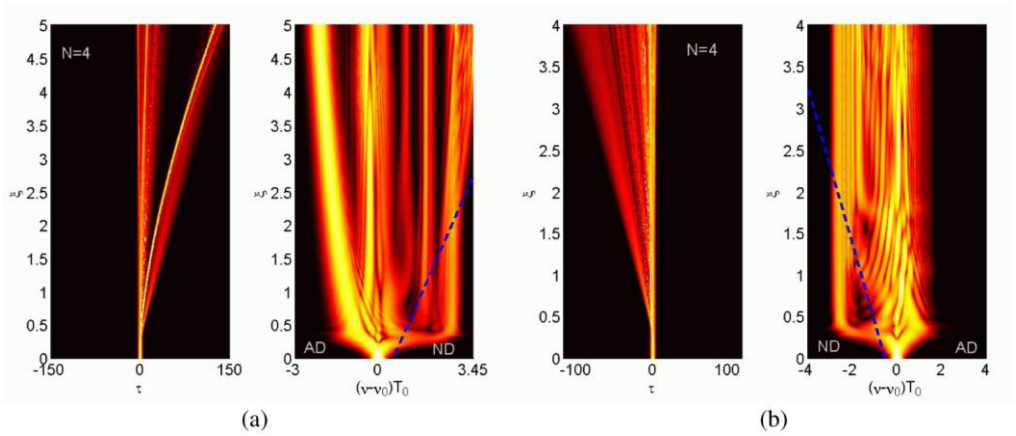

Fig. 11. (a) Temporal and (b) spectral evolution of an optical pulse launched in the normal dispersion (δ_2 = 0.5) domain close to the ZD wavelength with N = 4. The TOD parameter is positive (δ_3 = 0.05) for two left panes and negative (δ_3 = –0.05) for two right panes. Blue dotted lines show δ_2 as a function of frequency.

Figure 11 shows the temporal and spectral evolutions for N = 4 in the cases of positive (left) and negative δ_3. The blue dotted lines show how δ_2 varies as a function of frequency. For positive δ_3, the DW moves slower than the Raman soliton and appears behind the Raman soliton during propagation. However, because of the IPRS effect, the Raman soliton decelerates considerably. As a result, DW now catches up with the soliton, and the collision between them becomes unavoidable. This event is quite evident in Fig. 11(a). Because of XPM, new frequencies are generated and the spectrum of DW extends further towards the blue side, as seen in Fig. 11(a). The two spectrograms in Fig. 12 correspond to the two cases shown in Fig. 11. Here we see clearly how XPM interaction between the Raman soliton and DW creates new frequencies on the blue side. Physically, when Raman soliton is delayed enough that it begins to overlap with the DW, it traps the DW through XPM and forces it to move with it. As soliton is further red-shifted, a part of the DW shifts toward blue to ensure that the two move at the same speed. The situation is entirely different when δ_3 changes its sign to negative. In this case, the Raman soliton cannot shift toward the red side once its spectrum comes close to the ZD point, and a recoiling radiation appears beyond the ZD point in the normal-GVD domain. The temporal and spectral evolutions of the pulse shown in Fig. 11(b) present a clear evidence of a DW on the red side, as expected from theory [8,31]. From the temporal evolution in Fig. 11(b) and the spectrogram in Fig. 12(b) it can be noticed that Raman soliton hardly shifts from its original position in the time domain. The spectrogram confirms that DW travels faster than all other spectral components of the pulse but Raman soliton created by the blue component of the spectrum remain fixed in time domain. The numeric value of δ_3 is found to be one governing factor of the Raman soliton dynamics under these conditions.

#142719 - $15.00 USD Received 16 Feb 2011; accepted 4 May 2011; published 12 May 2011

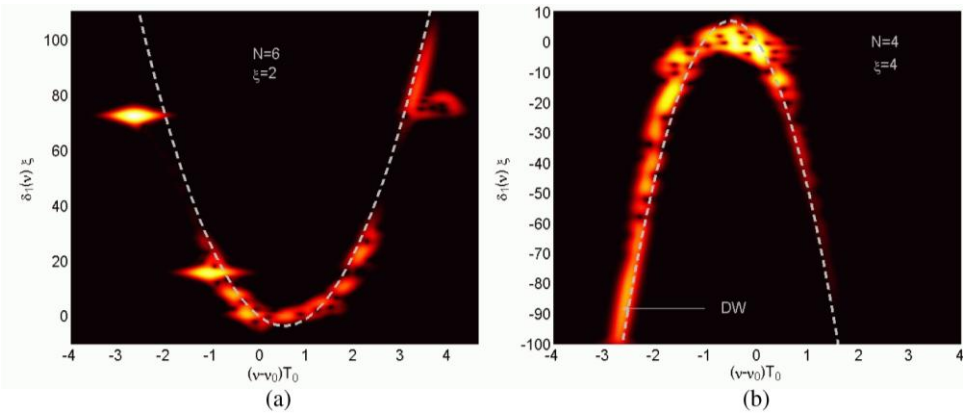

Fig. 12. (a) Spectrogram at a distance $\xi = 2$. for positive δ_3 and N = 6. (b) Spectrogram at a distance $\xi = 4$ under conditions of Fig. 11(b). The white dotted lines represent the delay.

4. Conclusions

In this paper we have focused on the supercontinuum process taking place when a femtoseond pulse is launched close to the ZD wavelength of a fiber. We allow the TOD to take both positive and negative values because both can occur in PCFs exhibiting two ZD wavelengths. Unusual dynamics of the Raman soliton is observed when the pulse is launched in the normal dispersion domain with a negative TOD. In this situation, the blue components of the pulse form a Raman soliton that moves faster than the signal pulse. However, as it is red shifted through IPRS, it gradually begins to decelerate. This deceleration stops when the soliton spectrum approaches the ZD point because of a cancellation of the Raman-induced spectral shift. In the time domain, the soliton trajectory bends and becomes vertical after the Raman shift is cancelled. However, the Raman soliton captures through XPM a part of the pulse spectrum on the red side that overlaps with it and force it to travel together. We have discussed in detail the influence of soliton order, input chirp and dispersion slope on the dynamics of Raman soliton.

Acknowledgement

The authors like to thank M. Komatsu for his help in formatting figures.

#142719 - $15.00 USD Received 16 Feb 2011; accepted 4 May 2011; published 12 May 2011